IEEE Access
Multidisciplinary | Rapid Review | Open Access Journal

Received 23 November 2023, accepted 2 December 2023, date of publication 5 December 2023,
date of current version 18 December 2023.

Digital Object Identifier 10.1109/ACCESS.2023.3339857

RESEARCH ARTICLE

A Region of Interest-Based Electrophysiological Source Imaging Technology and Its Applications in Analysis of Motor Imagery EEG Signals

YANPING WANG, XU ZHENG, AND NUO GAO
Department of Information and Electrical Engineering, Shandong Jianzhu University, Jinan 250101, China

Corresponding author: Nuo Gao (gaonuo@sdjzu.edu.cn)

This work was supported in part by the Shandong Provincial Natural Science Foundation under Grant ZR2022MF309; and in part by the Shandong Province Science and Technology Small and Medium-Sized Enterprise Innovation Ability Enhancement Project under Grant 2022TSGC2554.

This work involved human subjects or animals in its research. The authors confirm that all human/animal subject research procedures and protocols are exempt from review board approval.

ABSTRACT Electrophysiological source imaging (ESI) technology can map scalp potentials to the cerebral cortex, effectively address the shortcomings of low spatial resolution and the influence of volume conduction effects of electroencephalogram (EEG) signals. However, this mapping may lead to a significant increase in the amount of data, slow down data processing speed, and affect the real-time performance of the brain-computer interface (BCI) system. To address above issues, this paper proposes a region of interest (ROI) based ESI technology and applies it to the analysis of motor imagery electroencephalogram (MI-EEG) Signals. The proposed MI-EEG signal analysis method based on ROI-ESI technology first utilizes ESI technology to map scalp potential data to the interior of the cerebral cortex and obtain the source time series; Then, an ROI partitioning rule combining sensor position information is proposed to determine the ROI; Finally, feature extraction and classification of the source time series in the ROI are performed using filter bank CSP (FBCSP) and support vector machine (SVM). Experimental results show that the MI-EEG signal analysis method proposed in this paper can not only obtain accurate brain dipole activity information through scalp potential mapping, thereby accurately decoding EEG signals, but also eliminate source sequences unrelated to motor imagination through the division of interest regions, effectively improving signal processing speed, which makes it more suitable for online BCI applications.

INDEX TERMS Brain-computer interface (BCI), electrophysiological source imaging (ESI), region of interest (ROI), motor imagery electroencephalogram (MI-EEG).

I. INTRODUCTION

Brain-computer interface (BCI) is a communication system that facilitates communication and control between the brain and external devices bypassing the need for peripheral nerves and muscles [1]. Initially, the BCI system utilizes high-performance electrophysiological signal acquisition equipment to capture electroencephalogram (EEG) signals in real-time; Subsequently, the collected EEG signals are interpreted through various decoding algorithms; The final steps involves transforming the decoded results into control commands to enable the manipulation of external devices. As an emerging neural technology, BCI has demonstrated significant potential in enhancing the lives of patients with neurological muscle impairments caused by diseases such as stroke and spinal cord injury [2].

In BCI applications, EEG is increasingly favored by researchers due to its affordability, portability, and high temporal resolution. EEG signals are generally classified

The associate editor coordinating the review of this manuscript and approving it for publication was Humaira Nisar.

into two categories: evoked brainwaves (like P300 and steady-state visual evoked potentials) and spontaneous brain waves (like motor imagery). Spontaneous brainwaves, in contrast to evoked brainwaves, arise without external stimuli and are voltage changes in the scalp during central nervous system activity. They can effectively avoid fatigue caused by external stimuli in practical settings. Motor imagery, specially, generates different rhythmic changes in the motor sensory area of the brain by imagining limb movements, termed the sensorimotor rhythm (SMR) [3]. In SMR, the μ-rhythm (8-13Hz) and β-rhythm (13-30Hz) are most obvious. Imagining on the left hand movement results in the decrease in the μ-rhythm and β-rhythm energy of contralateral motor sensory area (a phenomenon as event related desynchronization or ERD) and an increase in the μ-rhythm and β-rhythm energy of ipsilateral motor sensory area (termed event related synchronization or ERS). Identifying these rhythmic changes using signal processing methods can facilitate the control of external devices.

The core of analyzing and decoding EEG signals is feature extraction and classification. Early research in this field primarily focused on applying experience for feature extraction and utilizing machine learning for classification to enhance the accuracy of decoding EEG signals. However, in recent developments, the method based on signal decomposition in feature extraction has been prevalent in the classification of motor imagery EEG signals, including empirical wavelet decomposition, discrete wavelet decomposition, variational mode decomposition and other types of decomposition ()() [4]. Sadiq et al. [5], [6] furthered the research on the empirical wavelet decomposition and variational mode decomposition, and proposed the multivariate empirical wavelet decomposition (MEWT) algorithm and the multivariate variational mode decomposition (MVMD) algorithm. The MEWT algorithm showed better classification accuracy and robustness as well as improved performance in cross-subject classification. The MVMD algorithm outperformed MEWT algorithm. Regarding classifier selection, convolutional neural networks gained prominence in EEG signal classification due to their excellent performance. In a comparative study of 11 popular classifiers by Sadiq et al. [7] indicated that the classification performance of convolutional neural networks surpassed machine learning algorithms.

Despite the increasing in the research and application of EEG-based BCI systems, limitations like poor spatial resolution and volume conduction effect prevent the current EEG signal analysis from achieving the necessary accuracy for the application of BCI technology [8]. Relevant studies have shown that increasing the number of scalp sensors can improve the spatial resolution of EEG signal but it does not completely address the problem of volume conduction [9].

Electrophysiological source imaging (ESI) is a method that deduces neural electrical activity based on non-invasive measurements such as EEG and magnetoencephalography (MEG). The fundamental principle of ESI is to counteract the effects of volume conduction or field propagation and reconstruct brain source activity from EEG and MEG signals [10]. It has been validated that ESI can solve the problem of poor spatial resolution and volume conduction of EEG. By establishing an accurate volume conduction model and mapping limited channel data onto the source dipoles in the cerebral cortex, more spatial information can be obtained [11].

In recent years, ESI technology has been studied in BCI application from multiple aspects such as complex motion decoding ability, decoding performance, application potential, and has shown great potential. Edelman et al. [12] applied ESI technology to decode wrist operations, categorizing four complex motion imagination tasks of the right hand. The results showed that the overall classification accuracy increased by 12.7% compared with traditional sensor-based methods. Mammone et al. [13] employed beamforming ESI and continuous wavelet transform to decode seven more refined upper limb movements, revealing that ESI technology has substantial potential in decoding fine upper limb movements. Edelman et al. [14] improved the spatial resolution of EEG through ESI, and developed a non-invasive framework based on EEG, which can continuously track random targets through brain-controlled robotic arms, and increase BCI control level by nearly 10%. Fang et al. [15] integrated ESI with hybrid feature convolutional neural networks, extracted features using continuous wavelet transform and optimal interested time. This integration has improved classification accuracy by about 2% through selecting the optimal interested time for each subject.

However, the process of ESI technology mapping scalp electrode data into the cerebral cortex can negatively increase the amount of data and reduce the speed of data processing, which will affect the real-time performance of the BCI system, limiting the application of ESI in BCI technology. To mitigate the limitations, Hou et al. [16] integrated the scout ESI with convolutional neural networks, created region of interest (ROI) with the help of scouts, extracted features from the scout's time series using Morlet wavelet method, and achieve a 14.4% increase in classification accuracy on certain datasets. This method reduces reliance on dipoles by establishing ROI, but the time for training is prolonged.

Given the significant potential of the ESI method in EEG signal analysis and the current existing of high computational complexity and prolonged computational time, this paper proposes an ROI based ESI technique and applies it to the analysis of MI-EEG Signals. The experimental results, both offline and online, reveal that the ROI partition rule combining sensor position information proposed in this paper can determine the best ROI on the basis of the analysis needs, effectively improve the signal processing speed on the premise of ensuring a high analysis accuracy, and is more suitable for the application of online BCI systems.

The subsequent part of the paper is structured as follows: Section II introduces the proposed ROI-ESI based MI-EEG signal analysis method, including the preprocessing of EEG signal, the forward and inverse problem of ESI, the ROI partition rule, the feature extraction and the classification. Section III delves into the experiment and discusses the results. Section IV concludes the paper.

II. MATERIALS AND METHODS

A. SYSTEM DESIGN

The system diagram of the proposed ROI-ESI based MI EEG signal analysis method is presented in Figure 1. The method consists of three components: EEG signal preprocessing, ROI based ESI technology, and feature extraction and classification. The process starts with preprocessing the signal to eliminate artifacts and noise, thereby improving the quality and reliability of the signal; Then, ROI-based ESI technology is used to map the preprocessed EEG signals to the cerebral cortex and divide the regions of interest, which includes solving the forward problem (calculating scalp potential from the cerebral cortex's dipole distribution based on a head model), the inverse problem (mapping scalp potential back to the cerebral cortex to determine dipole positions and numbers), and dividing the regions of interest. This paper proposes a ROI partition rule that incorporates sensor position. This rule divides regions of interest based on sensor position and signal characteristics. Subsequent analysis will only focus on the source sequence within the ROI. Therefore, the division of regions of interest can effectively reduce the amount of data processing and computational complexity. Finally, feature extraction and classification are performed on the source signals within the ROI, and the output of the classification results can complete the control of external devices. The following will provide a detailed discussion on each part of the proposed method in this paper.

B. SIGNAL PREPROCESSING

EEG signal is non-stationary and high susceptible to external influences. The process of recording EEG signals can result in a large number of artifacts, such as blink artifacts, electrocardiogram (ECG) artifacts, electromyogram (EMG) artifacts, power frequency interference, etc. For improved analytical results, it is necessary to perform denoising processing on the EEG signals. The preprocessing process of this paper includes bad channel replacement, spatial filtering, frequency domain filtering, independent component analysis (ICA).

1) BAD CHANNEL REPLACEMENT

In the recording process of EEG signals, the quality of source imaging can be seriously affected due to the loss or obvious errors in channel data, which happen because of poor contact between the EEG cap electrodes and the scalp. Obvious erroneous channels can be identified by visualizing the original EEG signal. To achieve the goal of data repair, interpolation can be utilized to replace the signal of the erroneous channel. In this paper, spherical splines interpolation method is employed to complete bad channel replacement [17]. This method projects the electrode position onto a unit sphere and then uses the signal of good channels to interpolate and replace the signal of faulty ones.

2) SPATIAL FILTERING

Common average reference (CAR) is a commonly used spatial filtering method has two advantages. Firstly, CAR can filter out the common mode component of EEG signals while retaining the characteristic information of each channel, thereby improving the signal-to-noise ratio; secondly, CAR shows relatively higher source imaging accuracy compared with single-electrode reference and double-electrode reference [18]. The calculation formula of the CAR method is shown in (1), and the potential of each channel is recalculated by subtracting the average value of all potentials.

$$C_i^{CAR}(t) = C_i(t) - \frac{1}{n}\sum_{i=1}^{n} C_i(t) \tag{1}$$

where $C_i(t)$ represents the original signal, $C_i^{CAR}(t)$ represents the signal after re-referencing, i represents the channel number, and n represents the total number of channels.

3) FREQUENCY DOMAIN FILTERING

This research focuses on the motor imagery EEG signals. The ERS and ERD phenomena related to MI mainly appear in the frequency band of 8-30Hz. In order to filter out interference from other frequency bands, this study employs a 4th-order Butterworth bandpass filter to perform frequency domain filtering on the EEG signals and filter out frequency components outside of 8-30Hz.

4) INDEPENDENT COMPONENT ANALYSIS (ICA)

Independent Component Analysis (ICA) is a multi-channel signal analysis method developed with blind source separation algorithm. ICA can effectively decompose multi-channel EEG data into spatially fixed and time-independent components, and effectively remove component components unrelated to motor imagery tasks, including blink artifacts, ECG artifacts, EMG artifacts. In this study, ICA is further used to remove irrelevant artifacts after filtering. For details of ICA algorithm, please refer to [19].

C. ESI TECHNOLOGY BASED ON REGIONS OF INTEREST

EEG is a comprehensive recording of the discharge activity of a large number of neuron clusters in the brain on the surface of the scalp. Ideally, the scalp electrode records brain source activity located below the electrode. However, due to the fact that various parts of the brain tissue (such as scalp, skull, cerebrospinal fluid, etc.) all have certain electrical conductivity, the actual source activity inside the brain will not only be transmitted upwards but also in other directions. This phenomenon is known as volume conduction effect [20]. Affected by volume conduction effects, the

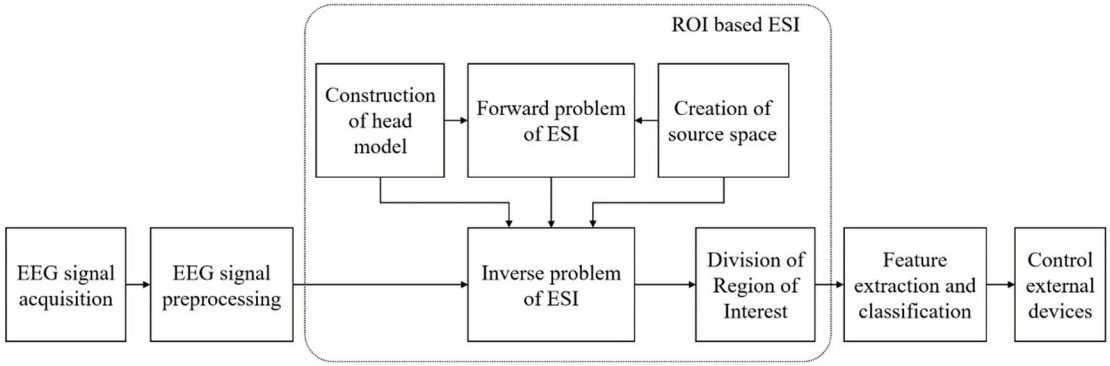

FIGURE 1. System block diagram of ESI-based ROI technology for EEG signal classification.

collected EEG signals are not directly corresponding to the signal of neuron clusters in the brain under the electrode, but are superimposed signals from multiple sources in the brain. Compared with magnetic resonance imaging, EEG cannot provide high-resolution structural images. Its spatial resolution is low, which limits the analysis and application of EEG. To overcome this disadvantage, a feasible method is to use recorded EEG signals to reconstruct the distribution pattern of signal sources inside the brain, which is called electrophysiological source imaging technology [21]. The electrophysiological source imaging process is shown in Figure 2 and includes two important concepts: forward problem and inverse problem. The forward problem aims to simulate the process of brain neural activity producing scalp potential and establish a lead matrix; The inverse problem aims to invert the activity of neural sources inside the brain to obtain information on source location, direction and strength.

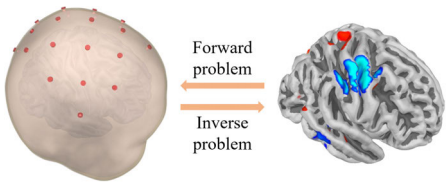

FIGURE 2. The forward and inverse problem diagrams of ESI technology.

1) FORWARD PROBLEM

The solution of the forward problem involves establishing a head model to calculate the lead matrix, constructing the relationship equation between the scalp surface and the source space, and calculating the scalp surface voltage based on the internal source signal of the brain. An accurate and effective head model is the basis for solving the forward problem. In order to improve the accuracy of solving the forward problem, the head model should mimic the geometry of the head as much as possible. At present, various head model schemes have been proposed, including three-shell concentric spheres [22], ellipsoids [23], and double concentric spheres [24]. With further research, researchers have found that different head tissues have different conductivities, and the different thicknesses and curvatures of individual skulls have a significant impact on source imaging. Utilizing a more realistic head model can result in a more accurate solution to the forward problem.

In this study, the public MRI template ''fsaverage'' is used to construct the head model. The ''fsaverage'' template is derived by scanning the real brain 40 times using MRI, and its image is shown in Figure 3(a). Then, the FreeSurfer software and the MNE-Python package are used to process structural MRI data to generate three-layer boundary element surfaces [25], including the inner surface of the skull, the outer surface of the skull, and the outer surface of the skin, as illustrated in Figure 3(b). The source space defines the position and direction of candidate sources. This study uses a subsampling method based on bilateral hemispheres to create a suitable source space on the white matter surface, as depicted in Figure 3(c), where purple dots represent candidate sources.

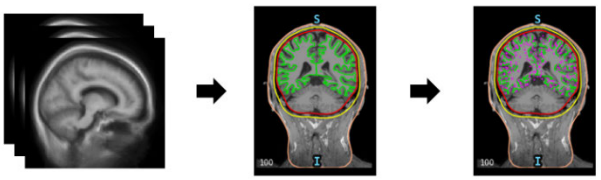

FIGURE 3. The process of solving a forward problem.

After creating the three-layer boundary element surface and source space, the researchers employ the boundary element method (BEM) to generate an isotropic three-shell realistic geometric head model with a conductivity ratio of 1:1/50:1, solves for the lead matrix, and establishes (2).

$$E_i = LS_i + N \tag{2}$$

$E_i \in \mathbb{R}^{n\times T}$ represents the preprocessed scalp EEG signal, $S_i \in \mathbb{R}^{m\times T}$ represents the EEG source signal, i represents the

number of experiments, $L \in \mathbb{R}^{n\times m}$ represents the lead matrix, and N represents the random noise signal.

2) INVERSE PROBLEM

Due to the fact that the number of scalp electrodes is far less than the number of EEG source dipoles, the mathematical problem of inferring the EEG source signal S_i from the scalp EEG data E_i is highly underdetermined. Introducing Tikhonov regularization is a classic way to solve such problems [26], which includes the minimum L1 norm method and the minimum L2 norm method. The L2 norm least squares method can be represented by (3) and (4):

$$\min_{S_i}(\|LS_i - E_i\|^2 + \lambda \|WS_i\|^2) \tag{3}$$

$$\hat{S}_i = L^T(LL^T + \lambda W)^{-1}E_i \tag{4}$$

λ is the regularization parameter, and W is the weighting matrix. There are many methods based on the minimum L2 norm regularization method, including minimum norm estimation [27], low-resolution electromagnetic tomography [28], and standardized low-resolution brain electrical tomography [29]. Among them, the standardized low-resolution brain electrical tomography method considers biological errors in the actual signal and assumes that biological errors are uniformly distributed throughout the brain. Therefore, it has better precise positioning and zero-error positioning and can obtain more spatial information. This article uses this method to solve the inverse problem and complete the source imaging process.

3) DIVISION OF THE ROI

The cerebral cortex is segmented into four lobes: frontal, temporal, parietal, and occipital, each responsible for various bodily functions. The parietal lobe, situated at the top of the head, plays a crucial role in the cerebral cortex, encompassing both motor and sensory functions. EEG signals related to motor imagination predominantly originate from the sensory motor cortex within the parietal lobe. To effectively isolate the relevant area, a partitioning rule for the ROI has been developed, which categorizes areas based on the location of sensors and the characteristics of the signals.

In an ideal scenario, when a scalp electrode is used, it primarily picks up the brain activity directly beneath it. However, due to the phenomenon known as volume conduction, the recorded signals are a mix from various sources. The influence of these sources on the EEG diminishes with distance from the electrode. Based on this, the suggested method for determining the ROI includes these steps:

(a) Pinpoint the exact coordinates of the scalp electrodes;

(b) Identify the brain dipole closest to each electrode;

(c) Expand outward from this dipole to define circular regions of different radii;

(d) Analyzing the EEG signals using source signals in regions of interest defined by different radii;

(e) Decide on the most effective ROI based on the outcomes of these analyses.

The delineation of the ROI is illustrated in Figure 4. In Figure 4(a), the somatosensory cortex is highlighted in blue, signifying its status as the primary focus of this study. Figure 4(b) details the methodology for identifying the dipole that is closest to the position of the scalp electrode. This involves calculating the distance between each dipole and the scalp electrode, followed by selecting the dipole that is in closest proximity to the electrode as the central point for outward expansion. Subsequently, Figure 4(c) depicts the designated ROIs in relation to the C3, Cz, and C4 scalp electrodes, each encompassing an expansion radius of 5mm.

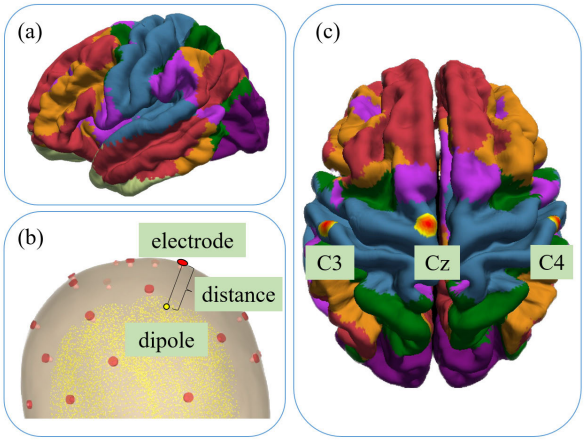

FIGURE 4. The process of dividing ROI. (a) Division of cerebral cortex region; (b) Central dipole determination process; (c) Example of ROI.

D. FEATURE EXTRACTION AND CLASSIFICATION

Feature extraction and classification play a crucial role in the entire BCI system, directly affecting the recognition rate of the entire BCI system. In 1990, Koles first proposed the common spatial pattern (CSP) method for EEG signal feature extraction [30]. Later, Romeser et al. applied the CSP algorithm to extract multi-channel EEG signal features and achieved ideal classification results, providing a theoretical basis for the subsequent application of CSP algorithms to BCI systems [31]. The CSP algorithm aims to construct an optimal spatial filter so that after the signal passes through the CSP filter, one class of signals has the maximum variance and the other class has the minimum variance, thereby maximizing the energy difference between the two classes of signals [32]. However, the CSP algorithm has certain limitations when processing multi-channel EEG signals containing a large amount of redundant information and noise. The FBCSP uses a mutual information-based optimal individual feature selection method on top of CSP to obtain relatively better classification accuracy [33]. In this study, the FBCSP algorithm is adopted to fulfill the feature extraction.

The diagram structure of the FBCSP algorithm is shown in Figure 5. In Figure 5, S_i^{ROI} represents the source time series of the ROI, W represents the projection matrix obtained by FBCSP calculation, f_i represents the extracted feature vector,

and i represents the number of experiments. The features can be calculated as (5).

$$\begin{cases} Z_i = W \times S_i^{ROI} \\ f_i = \log\left(\text{var}(Z_i)/\text{sum}(\text{var}(Z_i))\right) \end{cases} \tag{5}$$

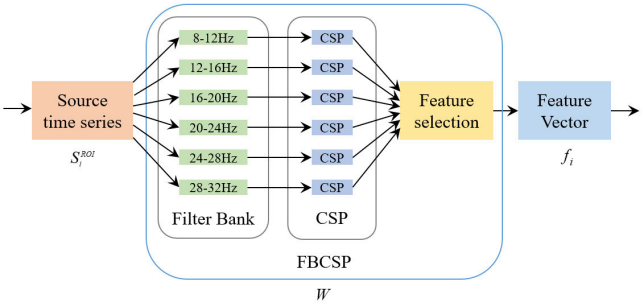

FIGURE 5. Calculation block diagram of FBCSP algorithm.

In this study, the support vector machine (SVM) algorithm is adopted to fulfill the classification. The SVM algorithm is a classification method that emerged in the 1990s. This method takes into account both empirical risk and structural risk minimization, making it possible to achieve better results when dealing with small sample training data and is widely used in EEG signal classification.

III. EXPERIMENTS AND DISCUSSION

A. OFFLINE EXPERIMENT

In order to verify the performance of the proposed method, the 4a dataset of the third BCI competition is selected for offline analysis. The 4a dataset contained two classes of motor imagery tasks: right hand movement imagination and right foot movement imagination. Subjects were required to sit in comfortable chair to complete the experiment. One motor imagery trial lasted for 3.5 seconds with a rest interval of 1.75-2.25 seconds between each trial during which the participants can relax. Five subjects were involved in this experiment labeled as aa, al, av, aw and ay. The EEG signals were recorded using a 118-channel electrode cap with a sampling frequency of 100Hz. Each subject performed 280 trials of motor imagery, in which 140 trials for right hand movement imagination and 140 trials for right foot movement imagination. The training and test data sizes of varied for each subject. The training data of five subjects are 168, 224, 84, 56, and 28 respectively, and the remaining data is used for testing.

1) DIVISION OF ROI

The study utilized two sets of ROI. The first set was delineated beginning at the scalp electrode and extending outward in a radius of 5mm, as depicted in Figure 6. The second set commenced at the scalp electrode as well, but expanded to a 10mm radius to define the ROI, as illustrated in Figure 7.

Table 1 lists the electrodes' names and numbers corresponding to these two ROI groups. In both Figure 6 and Figure 7, Figures (a) and (b) each represent a single scalp electrode. Starting with Figure (c), there is a progressive increase in the number of electrodes, culminating in Figure (h), which represents a cluster of seven scalp electrodes.

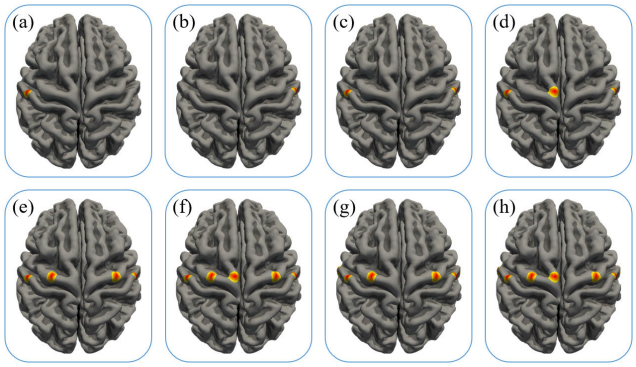

FIGURE 6. Division of ROI with an expansion radius of 5mm.

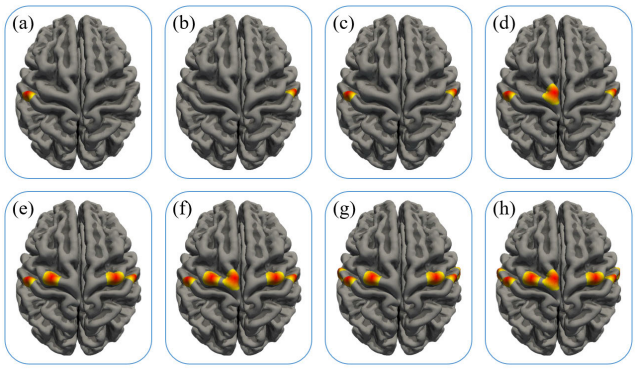

FIGURE 7. Division of ROI with an expansion radius of 10mm.

TABLE 1. Electrode descriptions corresponding to different ROI.

ROI label	Electrode	Quantity
(a)	C3	1
(b)	C4	1
(c)	C3, C4	2
(d)	C3, Cz, C4	3
(e)	C1, C2, C3, C4	4
(f)	C1, C2, Cz, C3, C4	5
(g)	C5, C3, C1, C2, C4, C6	6
(h)	C5, C3, C1, Cz, C2, C4, C6	7

2) ACCURACY OF DIFFERENT ROI

Building on the two sets of regions of interest discussed earlier, this study conducts offline experiments using the 4a dataset from the third BCI competition. Figure 8 illustrates the analysis accuracy for eight ROIs divided by a 5mm

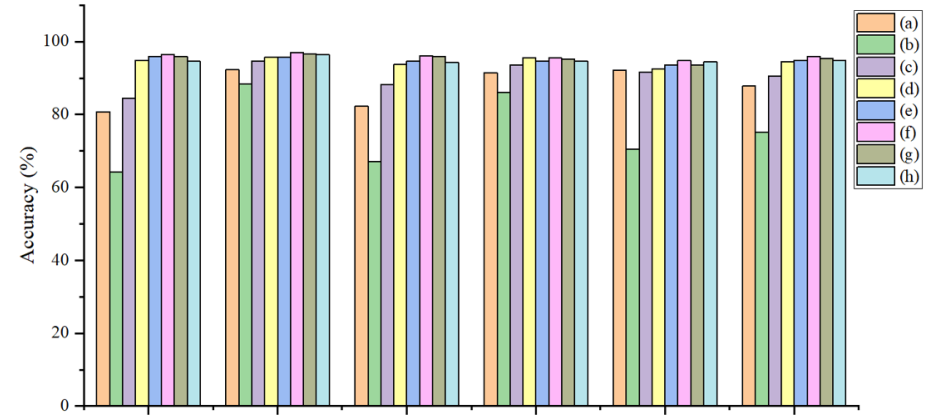

	aa	al	av	aw	ay	Avg
(a)	80.76	92.26	82.25	91.5	92.1	87.77
(b)	64.15	88.36	67.01	86	70.5	75.21
(c)	84.43	94.66	88.2	93.5	91.52	90.46
(d)	94.88	95.71	93.65	95.5	92.44	94.44
(e)	95.9	95.72	94.66	94.6	93.62	94.9
(f)	96.34	96.98	96.05	95.5	94.73	95.92
(g)	94.9	96.52	95.84	95.1	93.6	95.39
(h)	94.55	96.4	94.37	94.6	94.47	94.88

FIGURE 8. Classification accuracy of ROI with an expansion radius of 5mm.

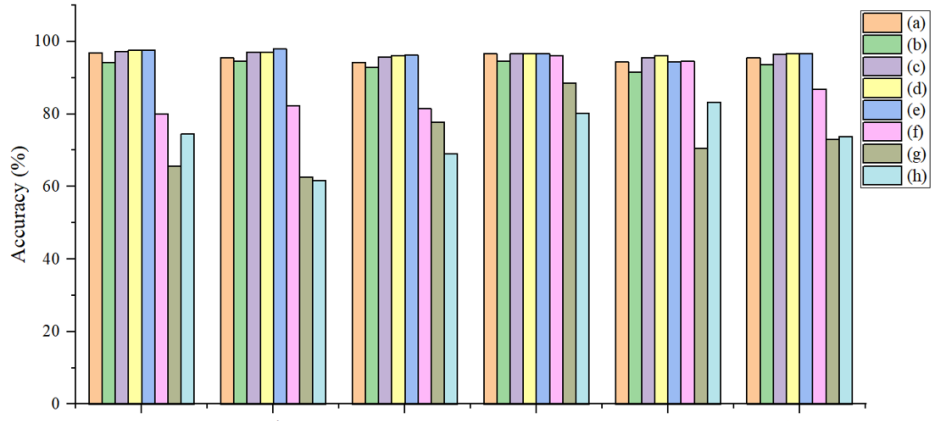

	aa	al	av	aw	ay	Avg
(a)	96.87	95.43	94.21	96.61	94.35	95.49
(b)	94.19	94.53	92.97	94.61	91.63	93.59
(c)	97.29	97.13	95.82	96.6	95.62	96.49
(d)	97.52	97.12	96.21	96.62	96.05	96.71
(e)	97.65	97.91	96.28	96.66	94.36	96.57
(f)	80.02	82.32	81.51	96.13	94.6	86.92
(g)	65.7	62.65	77.8	88.6	70.5	73.05
(h)	74.42	61.6	69.05	80.2	83.25	73.7

FIGURE 9. Classification accuracy of ROI with an expansion radius of 10mm.

expansion radius, as depicted in Figure 6. Similarly, Figure 9 presents the analysis accuracy for eight ROIs, each divided by a 10mm expansion radius, as shown in Figure 7. In both Figure 8 and Figure 9, the horizontal axis, labeled aa-ay, represents five participants, while 'Avg' denotes the average value. The vertical axis indicates the classification accuracy. Below the x-axis, there is a detailed data table corresponding to the histograms. This table's first five columns show the classification accuracy for each participant (aa-ay) across the eight regions of interest (a)-(h), and the final column displays the average classification accuracy. The legend's (a) to (h) correlate with the division of the eight regions of interest as outlined in Figures 6 and 7.

By analyzing the relationship between the accuracy and 8 ROIs (a-h) in Figure 8, following phenomenon can be seen: (1) Analysis accuracy of 5 subjects showed an overall increasing trend from ROI a to ROI h. (2) ROI a and ROI b have the lowest analysis accuracy among all regions of

interest, and ROI b is lower than ROI a; (3) The analysis accuracy tends to be stable from ROI f to ROI h, which is around 95%; (4) the ROI f has the highest average accuracy 95.92%.

The above phenomena show that:

(a) The expansion radius of 5mm is relatively small, less ROI contains less effective information. With the expansion of ROI and the increase of effective information, the analysis accuracy is gradually improved, which is also the reason of phenomenon (1) above.

(b) Since ROI a and ROI b both contain only one single electrode on one side of the brain (for example, a contains only C3 electrode and is located on the left side of the brain, b contains only C4 electrode and is located on the right side of the brain), and motor imagination, particularly the motor imagination of the left and right limbs, unilateral EEG signal cannot contain all the effective signals. Therefore, the analysis accuracies of ROI a and ROI b are low. Since the motor imagination of this dataset is right hand movement and right foot movement, due to the ERD phenomenon, it is easier to detect the feature changes of contralateral EEG signals, so the analysis accuracy of ROI a located on the left side of the brain is higher than that of ROI b located on the right side of the brain.

(c) When the ROI is extended to a certain extent (most useful information has been included), the analysis accuracy will plateau with the expansion of ROI, indicating that the ROI containing effective information has the best value. When ROI is too large, too much redundant information will affect the accuracy of signal analysis, resulting in a decline in analysis accuracy. This is also the significance of the ROI division proposed in this study.

Figure 9 is the analysis accuracy under 8 ROI divided by 10mm expansion radius, compared with Figure 8, Figure 9 depicts that:

(a) The analysis accuracy of all subjects showed a trend of an increase and then a decrease as the ROI changes. The highest analysis accuracy for all five subjects occurred in ROI d and ROI e.

(b) The analysis accuracies of ROI a-e are generally higher than that of ROI f-g.

(c) In Figure 9, the highest average accuracy was 96.71%, and the ROI at this time was ROI d, corresponding to three scalp electrodes (C3, Cz, C4); the highest average accuracy in Figure 8 was 95.92%, and the ROI at this time was ROI f, corresponding to five scalp electrodes (C3, C1, Cz, C2 and C4).

The three phenomena mentioned above indicate that when dividing the ROI with a 10mm expansion radius, as long as the electrode positions cover the left and right brains, the division of the ROI based on fewer electrodes can also contain most of the valid information. In this case, increasing the ROI will increase the redundant information contained in the source space, resulting in a decrease in classification accuracy. Therefore, the classification accuracy in Figure 9 shows an initial increase followed by a decrease with the highest classification accuracy appears in ROI d. The highest average classification accuracy in Figure 9 is 96.71%, which is 1 percentage point higher than that in Figure 8, indicating that using a 10mm expansion radius for ROI division has a slight advantage over using a 5mm expansion radius, and there is no order of magnitude difference between the two. At the same time, when using a 5mm expansion radius for ROI division, the highest classification accuracy appears in ROI f, corresponding to 5 scalp electrodes, while when using a 10mm expansion radius for ROI division, the highest classification accuracy appears in ROI d, corresponding to 3 scalp electrodes. This indicates that when dividing ROIs with a smaller radius expansion, more scalp electrode information is needed to obtain satisfactory classification results.

3) RESPONSE TIME OF DIFFERENT ROI

Response time can effectively reflect the communication efficiency of BCI system, and is also the core key to reflecting the smoothness of human-computer interaction. For high-real-time electrical signal acquisition systems such as EEG, the ideal response time is not more than 1 second in neuroregulatory scenarios and external interaction scenarios. The main function of the ROI division proposed in this study is to reduce the number of source signals, reduce the calculation amount, and improve the response time. In order to verify the influence of different ROIs on response time in this study, the motor imagination EEG signals of 5 subjects were analyzed and the average response time of 5 subjects was calculated based on the 16 ROIs divided by the previous two extended radii, as shown in Figure 10. During the response time testing, the test data for all subjects is independent of the training data. It can be seen from Figure 10 that whether the radius of expansion is 5mm or 10mm, from ROI a to ROI h, the response time increases rapidly with the expansion of ROI. The response time of ROI with an extended radius of 5mm increases from 0.504s to 1.007s, while the response time of ROI with an extended radius of 10mm increases from 0.810s to 1.365s. The ROI response time with an extended radius of 5mm is significantly lower than that with an extended radius of 10mm, with a reduction of 26%-37% in response time. In ROIs with extended radius of 10mm, only ROI a, b, and c have response times less than 1 second, while in ROIs with extended radius of 5mm, only ROI h has response times greater than 1 second. Obviously, for response time, the expansion radius of 5mm for the division of ROI is more advantageous. The above analysis shows that when designing brain-computer interface systems with high response time requirements, ROI f with an extended radius of 5mm can be selected as the ROI, while ROI d or ROI e with an extended radius of 10mm can be selected as the ROI for systems with high accuracy requirements.

4) PERFORMANCE COMPARISON BETWEEN THE PROPOSED METHOD AND THE CONTEMPORANEOUS METHODS

This study proposes a method that reduces the number of source signals by selecting ROIs to reduce computation and

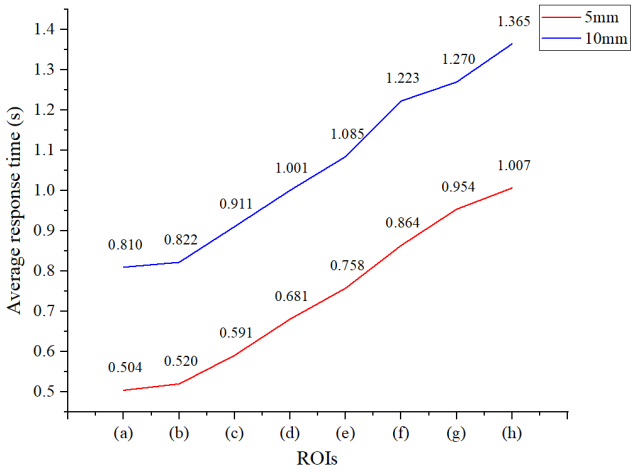

FIGURE 10. Average response time for different ROIs.

TABLE 2. Comparison of accuracy and response time of part ROIs.

Extended radius	ROI	Accuracy (%)	Response time (s)
5 mm	f	95.92	0.864
10 mm	d	96.71	1.001
10 mm	e	96.57	1.085

achieve fast response and high accuracy. To verify the effectiveness of the method, it has been compared with four other methods that are currently performing well. The four comparison methods are as follows: Peterson et al. [34] proposed the penalized time-frequency band common spatial patterns method (PTFBCSP) in 2019; Sadiq et al. [4] proposed the empirical wavelet transform-based imaginary amplitude and frequency component combined with least squares support vector machine method (EWT-IA-LS-SVM) in 2019; Molla et al. [35] proposed the neighborhood component analysis-based feature selection method (NCFS) in 2020; Fang et al. [15] proposed the ESI, continuous wavelet transform, and hybrid feature CNN-based method (ESI-CWT-CNN) in 2022. The comparative experiments were conducted using the third BCI competition 4a dataset. The experimental results are shown in Tables 3 and 4.

From Table 3, it can be observed that the average accuracy and standard deviation precision of the method proposed in this study outperforms the other four methods. For subject aa, the accuracy of all three ROI methods proposed in this article is higher than that of the other four methods, with a maximum accuracy of 97.65%. For subject av, whose accuracy is generally lower, the method proposed in this article can achieve a classification accuracy of 96%, slightly lower than that of the EWT-IA-LS-SVM method. From Table 4, it can be seen that the response time of ROI f with a 5mm expansion radius proposed in this article is much smaller than that of the other four methods. The response time of the two ROIs with a 10mm expansion radius is similar to that of the PTFBCSP method. It can also be seen that the response time of the two methods using EWT and CWT is much higher than that of the other two methods.

Based on the analysis of accuracy and response time, it can be concluded that the method proposed in this article has a similar response time to the PTFBCSP method, but the accuracy is improved by 5.5%-6.3%. Compared with the ESI-CWT-CNN method, which also uses ESI technology, the response time of the method proposed in this article is reduced by 67%-75%, indicating that the method proposed in this article can effectively reduce ESI calculation time and improve the real-time performance of BCI systems.

Nevertheless, some areas in this study need to be improved. First, the number of offline data sets utilized in this study is limited. In order to further verify the generalization ability of the proposed method, the offline analysis data needs to be expanded in the future research. For example, in order to verify the proposed multi-functional brain-computer interface framework, Sadiq et al. [36] used the BCI GigaDB dataset of large subjects, which contains motor imagery EEG recordings of 52 subjects. Stieger et al. [37] published a large-scale continuous MI-EEG dataset, which contains more than 600 hours of EEG recordings of 62 subjects. Secondly, good denoising effect is the key to improving the recognition accuracy. The denoising algorithm used in this paper is relatively traditional. At present, researchers have proposed a better MSPCA denoising algorithm. This algorithm combines wavelet with PCA, and the denoising effect is better than the original PCA algorithm. Thirdly, the feature extraction used in this paper is only for the time series of source space, which does not reflect the spatial characteristics of source imaging technology. At present, graphic features and geometric features are used in depression detection and epilepsy recognition, which is the focus of our follow-up research [38], [39].

B. ONLINE EXPERIMENT

In order to verify the online performance of the proposed method, the corresponding online experiments were conducted. The online experiments took place in the Laboratory of Novel Human-Machine Cooperative Intelligent Technology and Robot System of Shandong Jianzhu University, China. The acquisition of EEG signals was completed by the Neuracle NueSen W series 32-channel wireless EEG acquisition equipment. The electrode position is arranged according to the international 10-20 system, and the sampling frequency is 250Hz. A total of four subjects (labeled as s1, s2, s3, s4 in this paper) participated in the online experiments, all of whom were male students aged 20-26 years old of Shandong Jianzhu University. The online experiments were divided into two stages: training stage and testing stage. The training stage includes subjects getting familiar with the experimental process, motor imagination data collection, division of ROI and the training of classifier. And in testing stage, the subjects need to perform the virtual cursor online control experiment to test the online performance of the proposed method.

TABLE 3. Comparison of experimental accuracy (%) results.

Subject	PTFBCSP	EWT-IA-LS-SVM	NCFS	ESI-CWT-CNN	Proposed method in this paper		
					5mm-ROI f	10mm-ROI d	10mm-ROI e
aa	92.00	94.50	90.00	89.90	96.34	97.52	**97.65**
al	98.00	91.70	**98.93**	98.80	96.98	97.13	97.91
av	73.00	**97.20**	76.71	90.60	96.05	96.21	96.28
aw	94.00	95.60	**98.21**	95.60	95.50	96.62	96.66
ay	94.50	97.00	**97.14**	91.20	94.73	96.05	94.36
Avg	90.94	95.20	92.20	93.20	95.92	**96.71**	96.57
Std	8.86	2.01	8.37	3.43	0.85	**0.62**	1.41

TABLE 4. Comparison of experimental average accuracy and response time.

Method		Accuracy (%)	Response time (s)
PTFBCSP		90.94	1.032
EWT-IA-LS-SVM		95.20	2.105
NCFS		92.20	1.523
ESI-CWT-CNN		93.20	3.457
Proposed	5mm-ROI f	95.92	**0.864**
	10mm-ROI d	**96.71**	1.001
	10mm-ROI e	96.57	1.085

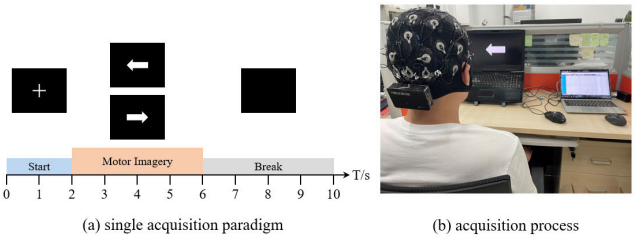

(a) single acquisition paradigm (b) acquisition process

FIGURE 11. EEG data acquisition process.

1) TRAINING STAGE

The training stage includes subjects getting familiar with the experimental process, motor imagination data collection, division of ROI and the training of classifier.

In the process of data collection, subjects were equipped with electrode caps and seated in a comfortable seat in front of a computer screen placed 50cm away, and then were instructed to perform corresponding motor imagination according to the screen prompts. Every subject performed motor imagination task 100 times, including 50 times left hand movement imagination and 50 times right hand movement imagination. Each MI process includes three stages: preparation stage, the motor imagination stage and the rest stage. The time flow of one MI process is shown in Figure 11(a). In preparation stage, a white cross appears in the center of the screen, signaling the subject to be prepare for motor imagination, which lasts for 2 seconds; In the motor imagination stage, the white cross was replaced by a white arrow to the left or right, and the subjects need to imagine left hand movement or right hand movement according to the arrow direction, which lasts for 4 seconds; In rest stage, the white cross disappeared and the screen appeared black, which is 4 seconds which provided the subjects a period to relax. Figure 11 (b) shows the real scene capture of the motor imagination stage.

The offline experimental analysis results in section III-A of this article show that the ROIs with better analysis accuracy are ROI c, d, e with 10mm expansion radii and ROI e, f, g, h with 5mm expansion radii. Therefore, in the online experiment, the above ROIs were selected as candidate ROIs for analysis. The analysis accuracy obtained by the four subjects under the above seven ROI divisions is shown in Figure 12. The left ordinate represents the accuracy, and its size is represented by a color histogram and the specific values are listed at the top of the histogram. The ordinate on the right side represents the average response time, which is represented by a black dot, and the specific number is presented above the black dot. From the figure, it can be seen that subject s1's highest analysis accuracy appears in ROI e-10mm, with a response time of 1.23 seconds. The second highest analysis accuracy appears in ROI g-5mm, with a response time of 0.95 seconds. Subject s2's highest analysis accuracy is ROI f-5mm, with a response time of 0.82 seconds. Subject s3's analysis accuracy is generally high, and the analysis accuracy reaches 94% in all three ROI cases. Among them, the shortest response time is ROI f-5mm. Subject s4 has the same highest analysis accuracy as s2, which appears in ROI f-5mm, with a response time of 0.81 seconds. Analyzing the accuracy and response time of the four subjects shows that the ROIs with high analysis accuracy and short response time all appear in the ROIs divided with a 5mm expansion radius. The reason may be attributed to more noise interference in laboratory data compared with that in BCI competition datasets selecting ROIs with smaller expansion radii can reduce noise interference and facilitate feature extraction and classification. Based on the analysis of accuracy and response time, the ROIs selected by the four subjects are: s1-ROI g-5mm, s2-ROI f-5mm, s3-ROI f-5mm, s4-ROI f-5mm.

2) TESTING STAGE

An online virtual cursor control experiment was used to conduct the online testing experiment, designed and completed by the researchers of the study. Python programming

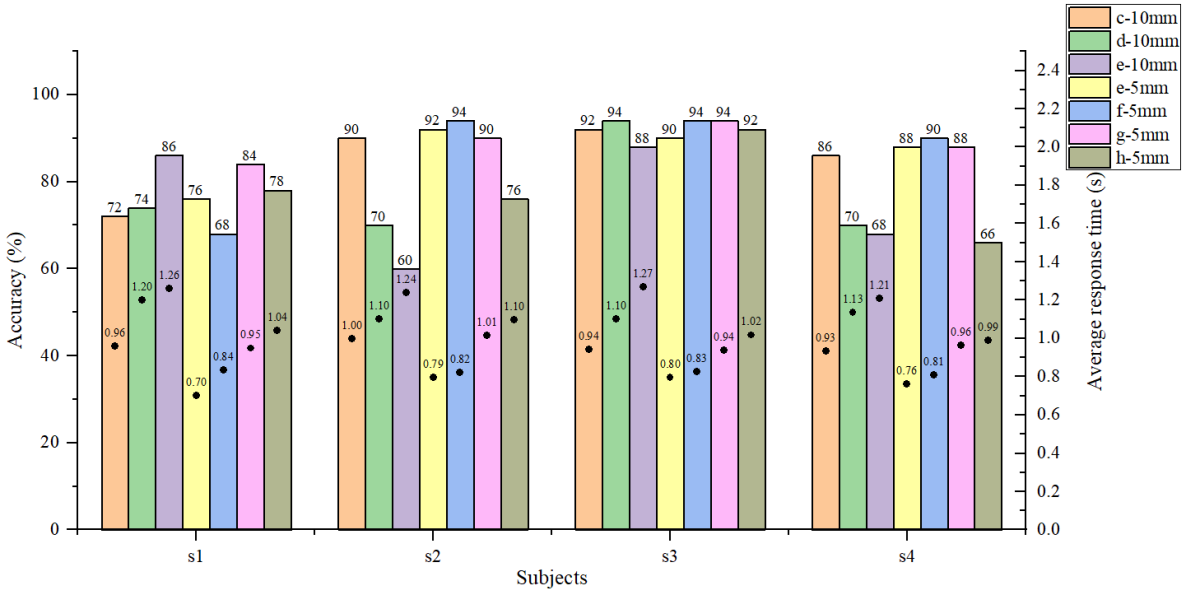

FIGURE 12. Analysis results of four subjects with different ROIs.

language was used to complete the software, and PyQt5 was used to complete the control interface.

The virtual cursor control interface is shown in Figure 13. In order to facilitate the observation of the subjects, the virtual cursor was replaced with a red ball. At the beginning of the experiment, a black rectangular object will randomly appear on left or right side of the screen, and the opposite side will be a dashed rectangle, as shown in Figure. 13 (a)(b). After the experiment starts, a red ball will drop in the middle top of the screen, and the ball will drop down at the default speed (1 s/grid). If the ball received instructions to move left or right, it moved one space to left or right, and if it did not receive instructions, it will continue drop. If the ball touches the black rectangular target on the left or right before falling to the bottom of the screen, it is marked as a success. Conversely, if the red ball touches the opposite dashed rectangle or falls to the bottom of the screen, it is marked as a failure.

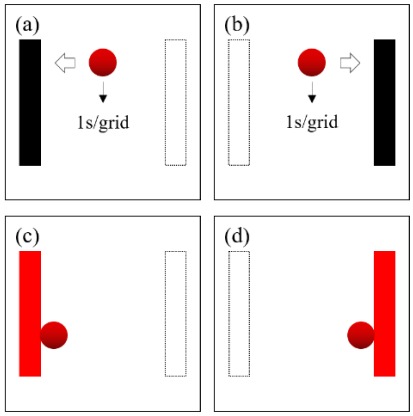

FIGURE 13. The interface of the online virtual cursor control experiment.

In this paper, the online virtual cursor control experiment is conducted on subject s3, which demonstrated the highest analysis accuracy in the training stage. The experiment is conducted in three separate rounds, with 20 ball touch experiments in each round, and the success rate of each round is calculated separately. The success rates of the three rounds for subject s3 were 90%, 85% and 90% respectively, with an average success rate of 88.33%. The shortest and longest time for the ball touching the rectangle was 7.2s and 14.8s respectively.

The success rates of online virtual cursor control experiments conducted in this paper are quite promising, with the success rate reaching above 88% and the control time remaining less than 15s. The results indicate that the ROI-based ESI technology proposed in this paper can effectively analyze and obtain the source signals that most relevant to scalp EEG, and through the analysis of source signals within ROI, a higher analysis accuracy can be obtained in a short response time. The success rate of online experiment is slightly lower than that of offline experiment because the real experiment process is easily affected by factors such as the concentration of subjects and external interference.

IV. CONCLUSION

This paper proposes a ROI-based ESI technique and applies it to the analysis of MI-EEG signals. The method encompasses several key steps. The initial step involves mapping the scalp electrode data to the cerebral cortex using the ESI technique, obtaining the source time series; then it proposes a ROI partitioning rule that combines sensor position information for the source space; finally, it uses FBCSP and SVM to complete feature extraction and classification. In order to verify the feasibility and effectiveness of the proposed method, a series

of offline and online experiments were carried out in this study.

The offline experiments were conducted on BCI Competition III 4a dataset and 5 subjects were involved in the experiments. The corresponding experiments were conducted from the aspects of ROI division, the impact of different ROI divisions on analysis accuracy, response time and system performance. The experimental results show that the method proposed in this paper can achieve a relatively high analysis accuracy (>95%) whether 5mm is used as the extended radius or 10mm is used as the extended radius to divide the ROI. If considering the response time at the same time, the balance between the analysis accuracy and the response time can be achieved by dividing the ROI with the extended radius of 5mm (accuracy>95%, response time<1s). At this time, at least 5 electrodes on both sides of the brain must be considered when dividing the ROI with 5mm radii. The online experiment was conducted in the Laboratory of New Human-Computer Cooperative Intelligent Technology and Robot System of Shandong Jianzhu University. After the data training stage, subject s3 (who has the best analysis effect) was selected for the virtual cursor control online experiment. The accuracies of three rounds online experiments were all higher than 88%, and the time of each cursor touching experiment was between 7.2s-14.8s.

Offline and online experimental results show that the proposed method can not only accurately map low spatial resolution EEG signals to the cerebral cortex by ESI technology, but also can partition the most effective regions of interest, eliminate irrelevant source information, effectively reduce data processing and reduce response time by using the ROI partitioning rules proposed in this paper. The higher accuracy and lower response time make the method proposed in this paper more suitable for online experiments. Our subsequent work is to apply the method proposed in this paper to the control of actual equipment, such as manipulators, wheelchairs, etc.

REFERENCES

[1] F. Lotte, L. Bougrain, A. Cichocki, M. Clerc, M. Congedo, A. Rakotomamonjy, and F. Yger, "A review of classification algorithms for EEG-based brain–computer interfaces: A 10 year update," *J. Neural Eng.*, vol. 15, no. 3, Apr. 2018, Art. no. 031005, doi: 10.1088/1741-2552/aab2f2.

[2] J. Fu, S. Chen, and J. Jia, "Sensorimotor rhythm-based brain–computer interfaces for motor tasks used in hand upper extremity rehabilitation after stroke: A systematic review," *Brain Sci.*, vol. 13, no. 1, p. 56, Dec. 2022, doi: 10.3390/brainsci13010056.

[3] Z. Yu, W. Chen, and T. Zhang, "Motor imagery EEG classification algorithm based on improved lightweight feature fusion network," *Biomed. Signal Process. Control*, vol. 75, May 2022, Art. no. 103618, doi: 10.1016/j.bspc.2022.103618.

[4] M. T. Sadiq, X. Yu, Z. Yuan, Z. Fan, A. U. Rehman, G. Li, and G. Xiao, "Motor imagery EEG signals classification based on mode amplitude and frequency components using empirical wavelet transform," *IEEE Access*, vol. 7, pp. 127678–127692, 2019, doi: 10.1109/ACCESS.2019.2939623.

[5] M. T. Sadiq, X. Yu, Z. Yuan, F. Zeming, A. U. Rehman, I. Ullah, G. Li, and G. Xiao, "Motor imagery EEG signals decoding by multivariate empirical wavelet transform-based framework for robust brain–computer interfaces," *IEEE Access*, vol. 7, pp. 171431–171451, 2019, doi: 10.1109/ACCESS.2019.2956018.

[6] M. T. Sadiq, X. Yu, Z. Yuan, M. Z. Aziz, N. U. Rehman, W. Ding, and G. Xiao, "Motor imagery BCI classification based on multivariate variational mode decomposition," *IEEE Trans. Emerg. Topics Comput. Intell.*, vol. 6, no. 5, pp. 1177–1189, Oct. 2022, doi: 10.1109/TETCI.2022.3147030.

[7] M. T. Sadiq, H. Akbari, S. Siuly, Y. Li, and P. Wen, "Alcoholic EEG signals recognition based on phase space dynamic and geometrical features," *Chaos, Solitons Fractals*, vol. 158, May 2022, Art. no. 112036, doi: 10.1016/j.chaos.2022.112036.

[8] M.-A. Li, Y.-X. Dong, Y.-J. Sun, J.-F. Yang, and L.-J. Duan, "Subject-based dipole selection for decoding motor imagery tasks," *Neurocomputing*, vol. 402, pp. 195–208, Aug. 2020, doi: 10.1016/j.neucom.2020.03.055.

[9] V. Shenoy Handiru, A. P. Vinod, and C. Guan, "EEG source imaging of movement decoding: The state of the art and future directions," *IEEE Syst., Man, Cybern. Mag.*, vol. 4, no. 2, pp. 14–23, Apr. 2018, doi: 10.1109/MSMC.2017.2778458.

[10] A. Sohrabpour and B. He, "Exploring the extent of source imaging: Recent advances in noninvasive electromagnetic brain imaging," *Current Opinion Biomed. Eng.*, vol. 18, Jun. 2021, Art. no. 100277, doi: 10.1016/j.cobme.2021.100277.

[11] C. M. Michel and D. Brunet, "EEG source imaging: A practical review of the analysis steps," *Frontiers Neurol.*, vol. 10, p. 325, Apr. 2019, doi: 10.3389/fneur.2019.00325.

[12] B. J. Edelman, B. Baxter, and B. He, "EEG source imaging enhances the decoding of complex right-hand motor imagery tasks," *IEEE Trans. Biomed. Eng.*, vol. 63, no. 1, pp. 4–14, Jan. 2016, doi: 10.1109/TBME.2015.2467312.

[13] N. Mammone, C. Ieracitano, and F. C. Morabito, "A deep CNN approach to decode motor preparation of upper limbs from time–frequency maps of EEG signals at source level," *Neural Netw.*, vol. 124, pp. 357–372, Apr. 2020, doi: 10.1016/j.neunet.2020.01.027.

[14] B. J. Edelman, J. Meng, D. Suma, C. Zurn, E. Nagarajan, B. S. Baxter, C. C. Cline, and B. He, "Noninvasive neuroimaging enhances continuous neural tracking for robotic device control," *Sci. Robot.*, vol. 4, no. 31, Jun. 2019, Art. no. eaaw6844, doi: 10.1126/scirobotics.aaw6844.

[15] T. Fang, Z. Song, G. Zhan, X. Zhang, W. Mu, P. Wang, L. Zhang, and X. Kang, "Decoding motor imagery tasks using ESI and hybrid feature CNN," *J. Neural Eng.*, vol. 19, no. 1, Feb. 2022, Art. no. 016022, doi: 10.1088/1741-2552/ac4ed0.

[16] Y. Hou, L. Zhou, S. Jia, and X. Lun, "A novel approach of decoding EEG four-class motor imagery tasks via scout ESI and CNN," *J. Neural Eng.*, vol. 17, no. 1, Feb. 2020, Art. no. 016048, doi: 10.1088/1741-2552/ab4af6.

[17] F. Perrin, J. Pernier, O. Bertrand, and J. F. Echallier, "Spherical splines for scalp potential and current density mapping," *Electroencephalogr. Clin. Neurophysiol.*, vol. 72, no. 2, pp. 184–187, Feb. 1989, doi: 10.1016/0013-4694(89)90180-6.

[18] K. Mahjoory, V. V. Nikulin, L. Botrel, K. Linkenkaer-Hansen, M. M. Fato, and S. Haufe, "Consistency of EEG source localization and connectivity estimates," *NeuroImage*, vol. 152, pp. 590–601, May 2017, doi: 10.1016/j.neuroimage.2017.02.076.

[19] S. Makeig, A. J. Bell, T. Jung, and T. Sejnowski, "Independent component analysis of electroencephalographic data," in *Proc. Neural Inf. Process. Syst.*, Nov. 1995, pp. 1–7. [Online]. Available: https://www.semanticscholar.org/paper/Independent-Component-Analysis-of-Data-Makeig-Bell/f61237db63fb1616fe2c9ff8a81d863a72500a37

[20] M. Hassan and F. Wendling, "Electroencephalography source connectivity: Aiming for high resolution of brain networks in time and space," *IEEE Signal Process. Mag.*, vol. 35, no. 3, pp. 81–96, May 2018, doi: 10.1109/MSP.2017.2777518.

[21] B. He, A. Sohrabpour, E. Brown, and Z. Liu, "Electrophysiological source imaging: A noninvasive window to brain dynamics," *Annu. Rev. Biomed. Eng.*, vol. 20, no. 1, pp. 171–196, Jun. 2018, doi: 10.1146/annurev-bioeng-062117-120853.

[22] H. Hallez, B. Vanrumste, R. Grech, J. Muscat, W. De Clercq, A. Vergult, Y. D'Asseler, K. P. Camilleri, S. G. Fabri, S. Van Huffel, and I. Lemahieu, "Review on solving the forward problem in EEG source analysis," *J. NeuroEng. Rehabil.*, vol. 4, no. 1, p. 46, Nov. 2007, doi: 10.1186/1743-0003-4-46.

[23] F. Kariotou, "Electroencephalography in ellipsoidal geometry," *J. Math. Anal. Appl.*, vol. 290, no. 1, pp. 324–342, Feb. 2004, doi: 10.1016/j.jmaa.2003.09.066.

[24] F. Vatta, P. Bruno, and P. Inchingolo, "Multiregion bicentric-spheres models of the head for the simulation of bioelectric phenomena," *IEEE Trans. Biomed. Eng.*, vol. 52, no. 3, pp. 384–389, Mar. 2005, doi: 10.1109/tbme.2004.843258.
[25] A. Gramfort, "MEG and EEG data analysis with MNE-Python," *Frontiers Neurosci.*, vol. 7, p. 267, Jan. 2013. [Online]. Available: https://www.frontiersin.org/articles/10.3389/fnins.2013.00267
[26] R. Grech, T. Cassar, J. Muscat, K. P. Camilleri, S. G. Fabri, M. Zervakis, P. Xanthopoulos, V. Sakkalis, and B. Vanrumste, "Review on solving the inverse problem in EEG source analysis," *J. NeuroEng. Rehabil.*, vol. 5, no. 1, p. 25, Nov. 2008, doi: 10.1186/1743-0003-5-25.
[27] M. S. Hämäläinen and R. J. Ilmoniemi, "Interpreting magnetic fields of the brain: minimum norm estimates," *Med. Biol. Eng. Comput.*, vol. 32, no. 1, pp. 35–42, Jan. 1994, doi: 10.1007/BF02512476.
[28] R. D. Pascual-Marqui, C. M. Michel, and D. Lehmann, "Low resolution electromagnetic tomography: A new method for localizing electrical activity in the brain," *Int. J. Psychophysiol.*, vol. 18, no. 1, pp. 49–65, Oct. 1994, doi: 10.1016/0167-8760(84)90014-X.
[29] R. Pascual-Marqui. (2002). *Standardized Low-Resolution Brain Electromagnetic Tomography (sLORETA): Technical Details*. Methods and Findings in Experimental and Clinical Pharmacology. Accessed: Jun. 20, 2023. [Online]. Available: https://www.semanticscholar.org/paper/Standardized-low-resolution-brain-electromagnetic-Pascual-Marqui/6908a6e13a1aff03007d8478129403dbcbd6f348
[30] Z. J. Koles, M. S. Lazar, and S. Z. Zhou, "Spatial patterns underlying population differences in the background EEG," *Brain Topography*, vol. 2, no. 4, pp. 275–284, Jun. 1990, doi: 10.1007/bf01129656.
[31] H. Ramoser, J. M'uller-Gerking, and G. Pfurtscheller, "Optimal spatial filtering of single trial EEG during imagined hand movement," *IEEE Trans. Rehabil. Eng.*, vol. 8, no. 4, pp. 441–446, Dec. 2000, doi: 10.1109/86.895946.
[32] D. Li, H. Zhang, M. S. Khan, and F. Mi, "A self-adaptive frequency selection common spatial pattern and least squares twin support vector machine for motor imagery electroencephalography recognition," *Biomed. Signal Process. Control*, vol. 41, pp. 222–232, Mar. 2018, doi: 10.1016/j.bspc.2017.11.014.
[33] K. K. Ang, Z. Y. Chin, C. Wang, C. Guan, and H. Zhang, "Filter bank common spatial pattern algorithm on BCI competition IV datasets 2a and 2b," *Frontiers Neurosci.*, vol. 6, p. 39, Mar. 2012, doi: 10.3389/fnins.2012.00039.
[34] V. Peterson, D. Wyser, O. Lambercy, R. Spies, and R. Gassert, "A penalized time-frequency band feature selection and classification procedure for improved motor intention decoding in multichannel EEG," *J. Neural Eng.*, vol. 16, no. 1, Jan. 2019, Art. no. 016019, doi: 10.1088/1741-2552/aaf046.
[35] Md. K. I. Molla, A. A. Shiam, Md. R. Islam, and T. Tanaka, "Discriminative feature selection-based motor imagery classification using EEG signal," *IEEE Access*, vol. 8, pp. 98255–98265, 2020, doi: 10.1109/ACCESS.2020.2996685.
[36] M. T. Sadiq, X. Yu, Z. Yuan, M. Z. Aziz, S. Siuly, and W. Ding, "Toward the development of versatile brain–computer interfaces," *IEEE Trans. Artif. Intell.*, vol. 2, no. 4, pp. 314–328, Aug. 2021, doi: 10.1109/TAI.2021.3097307.
[37] J. R. Stieger, S. A. Engel, and B. He, "Continuous sensorimotor rhythm based brain computer interface learning in a large population," *Sci. Data*, vol. 8, no. 1, p. 98, Apr. 2021, doi: 10.1038/s41597-021-00883-1.
[38] H. Akbari, M. T. Sadiq, M. Payan, S. S. Esmaili, H. Baghri, and H. Bagheri, "Depression detection based on geometrical features extracted from SODP shape of EEG signals and binary PSO," *Traitement du Signal*, vol. 38, no. 1, pp. 13–26, Feb. 2021, doi: 10.18280/ts.380102.
[39] H. Akbari, M. T. Sadiq, N. Jafari, J. Too, N. Mikaeilvand, A. Cicone, and S. Serra-Capizzano, "Recognizing seizure using Poincaré plot of EEG signals and graphical features in DWT domain," *Bratislava Med. J.*, vol. 124, no. 1, pp. 12–24, 2022, doi: 10.4149/bll_2023_002.

YANPING WANG received the B.S. degree in engineering from Shandong Jianzhu University, Jinan, China, in 2020, where he is currently pursuing the M.S. degree with the School of Information and Electrical Engineering.

His current research interests include EEG signal processing, brain–computer interface, and machine learning.

XU ZHENG received the B.S. degree in engineering from Shandong Jianzhu University, Jinan, China, in 2021, where he is currently pursuing the M.S. degree with the School of Information and Electrical Engineering.

His current research interests include EEG signal processing, brain–computer interface, and deep learning.

NUO GAO received the M.S. degree from the Department of Electrical Engineering, Shandong University, Jinan, China, in 2000, and the Ph.D. degree from the Department of Electrical Engineering, Zhejiang University, Zhejiang, China, in 2005.

From 2006 to 2007, she was a Postdoctoral Fellow with the Department of Biomedical Engineering, University of Minnesota. She has published dozens of academic papers and participated in several projects of Shandong Provincial Department of Science and Technology. Her research interests include bioelectrical signal processing, brain–computer interface systems, and rehabilitation robot systems. She has been the Elsevier's Most Cited Chinese Researchers for three consecutive years, from 2015 to 2017.